

# LF signal injection for earth-fault localization in unearthed distribution network

Nina Stipetic, Bozidar Filipovic-Grcic, Igor Ziger

**Abstract** – Unearthed neutral is often used in industrial networks, which require continuous power supply, and in distribution networks where the network capacitive current is not too high; or it is uneconomical to move to compensated grounding. Unearthed networks can remain in operation during an earth-fault, but fast determination of the faulty line is the key for prevention of further fault escalation. Signal injection is one of the fault location methods often used in LV unearthed networks. The possibility of application of this method in MV networks is dependent on how to inject the signal into unearthed phases with voltages ranging from 10 to 35 kV. This paper presents the signal injection circuit, which consist of three inductive voltage transformers (IVTs). The specifics of IVT design for signal injection are discussed. The application of the LF signal injection during an earth-fault was simulated on the model of an unearthed distribution network in EMTP. An intermittent fault and ring-type network connection were considered as possible cases.

**Keywords:** unearthed network, earth-fault, low-frequency signal injection, inductive voltage transformer

## I. INTRODUCTION

The grounding method is important for the reliability of the power system networks' operation. Depending on the grounding method, different waveforms, and amplitudes of overvoltages and fault currents may appear during single-phase-to-ground faults. In unearthed networks, the earth-fault current closes through systems' capacitances to ground, which does not lead to a high fault current and there is no need for fault interruption. Even though the unearthed network can remain operating after an earth-fault, locating the faulty line is important to minimize the overvoltage stress in healthy phases and to prevent the secondary fault, which would require switching [1]. Single-phase faults are the most frequent in distribution networks, representing 50-90 % of all faults [2],[3]. There is still no commonly accepted, reliable and efficient method for earth fault location in distribution networks [2], [4] since it depends on fault type, grounding method and network characteristics; and the combinations are numerous.

In practice, the earth-fault directional overcurrent protection (67N) is accepted as adequate, off-the-shelf solution for ungrounded networks. It requires numerical relays and appropriate current transformers optimally placed along feeders

together with communication infrastructure. It is based on the fundamental-frequency phasor measurement and zero-sequence voltage and current calculation. The experiences related to it are spurious tripping due to unbalances and missing to trip due to sensitivity limitation and very low zero-sequence current in small networks and on short cables. If the directional earth-fault protection is not used, the fault detection is usually done by zero-sequence voltage measurement for earth-fault indication and sequential disconnection of feeders for fault clearing.

An extensive research and development of new methods for earth-fault location in distribution networks are continuously done. Most of them are based on either centralized or decentralized measurements of fundamental-frequency current and voltage, impedance and fault distance calculation [2],[5]-[8]. Research has also been done on the travelling-wave-based method that theoretically yields good results. However, it is challenging for practical application due to the complexity of MV networks and need for sophisticated measurement equipment with high sampling rates. Transient and high frequency measurement methods share the same measurement problem [10]-[15]. The artificial intelligence-based methods recently gained much attention, but example of real-life application is difficult to find [16-18]. Another known method is a signal injection method. It implies test signal injection into the network and tracking it throughout the system to find the faulty line, since the test signal closes its path through the fault [19-22], or calculation of fault distance based on the injected signal. In [4], it is stated that the injection method was confirmed in MV practice, but the application was possible for compensated networks only. Nevertheless, in [23] it was shown that the signal injection in unearthed MV network is possible on an example of a small, industrial, radial cable network. This paper shows further possibilities of signal injection method application into larger, mixed cable-overhead line distribution network. The paper discusses the modifications of the IVT that can be done to enable the injection into larger networks.

### A. Signal injection circuit for MV unearthed networks

In isolated MV networks fed by a transformer with a delta winding, the neutral is not accessible. In that case, it is possible to use the configuration of three single-phase insulated IVTs to connect the signal generator between the artificial neutral and ground, as depicted in Fig.1. A signal generator injects current through primary windings of IVTs which are grounded over a capacitor to avoid current being shunted. The secondaries of three-winding voltage transformers are used for connection of LV measurement equipment, which was modelled as an impedance of 53  $\Omega$  to get the rated burden. The tertiary is delta-

---

N. Stipetic and B. Filipovic-Grcic are with University of Zagreb, Faculty of Electrical Engineering and Computing, 10000 Zagreb, Croatia (e-mail of corresponding author: [nina.stipetic@fer.hr](mailto:nina.stipetic@fer.hr))

I. Ziger is with Koncar Instrument Transformers Inc., 10000 Zagreb, Croatia (e-mail: [igor.ziger@koncar-mjt.hr](mailto:igor.ziger@koncar-mjt.hr))

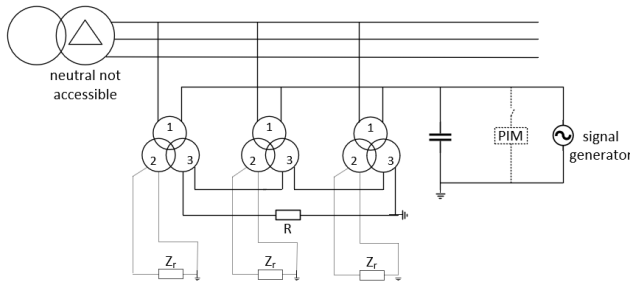


Fig. 1. Schematic preview of signal injection into isolated MV network using the primary windings of IVTs

connected and loaded with resistor for dampening the ferroresonance phenomena [24]. The circuit is similar to the connection circuit of the permanent insulation monitor (PIM), which uses DC injection for calculation of total network resistance. The PIM usually has several predefined values for injection, for example 20, 40, 60 and 80 V<sub>DC</sub>.

This research focuses on sinusoidal test signal since the idea is to use current transformers or Rogowski coils for injected signal detection. Low frequency (LF) is used to maximize the capacitive reactance of healthy lines and increase the probability for the test LF sine wave signal to close path through resistance at the fault location. Increasing the injection signal magnitude facilitates the detection by current sensors. Induced voltage in IVT is described by the following equation:

$$E_{rms} = 4.44 \cdot N \cdot f \cdot \phi_{max} \rightarrow \phi_{max} = \frac{E_{rms}}{4.44 \cdot f \cdot N} \quad (1)$$

where  $\phi$  is the core magnetic flux,  $E$  is the induced voltage and  $N$  is the number of turns. Observing the equation (1) it is clear that changing the ratio  $E/f$  leads to a change in the flux  $\phi$ . Increase of the flux over the knee point of the current-flux curve will lead to core saturation which increases the current through the primary winding and this should generally be avoided. Hence, the IVT is the key piece of equipment for the application of signal injection method in unearthened networks. Signal parameters should be chosen optimally for injection into the network and, if needed, the IVT design should be adjusted to avoid the unwanted saturations.

### B. Distribution network model

To test the method in distribution network, an unearthened 10 kV distribution network similar to distribution network presented in [2] was modelled. The network equivalent is modelled as ideal 132 kV voltage source behind impedance based on 250 MVA short-circuit power. The main transformer and load transformers are delta connected on the MV side and they are represented by low-frequency models available in EMTP library. The network is mixed cable-OHL network with radial feeders and one ring connection. The cables and overhead lines were modelled as PI equivalents including their conductances. Simulations were done for two cases – with and without the ring connection. The network scheme with marked fault locations is given in Fig.2. For signal injection, a circuit from Fig. 1 was modelled in EMTP, as outlined in Fig. 2. A real 10 kV IVT including the magnetization curve is modelled. The

group of three single-pole insulated IVTs intended for unearthened networks usually have a resistor in delta connected tertiary circuit for ferroresonance mitigation. For efficient ferroresonance damping, a resistance that consumes 25 W at 100 V per kilogram of the IVT core is normally used [24], [25]. The mass of a core of 10 kV IVT does not exceed 13 kg. Hence a resistor of 30  $\Omega$  for a consumption of 325 W at 100 V is connected to the close the delta connection circuit of tertiary windings. The data used for modelling is given in the Appendix.

## II. INITIAL SIMULATIONS

The initial simulations of earth-faults and signal injection are performed to check if the currents and voltages are behaving as expected. The frequency of injected signal is chosen to be 2.5 Hz, to follow the practice in LV systems. Initial simulations have shown that 2.5 Hz is a reasonable choice. Choosing another frequency is possible. However, due to equation (1), another frequency will affect the flux in the core and the signal generator voltage should be adjusted to avoid the transformer saturation. The transformer core design could be optimized for chosen parameters of injected signal that are to be used in some network. Different frequency will affect the most the injected signal distribution in the network. The detection limit regarding the fault resistance will drop with the increase of injected signal frequency.

Firstly, the DC injection for total network resistance calculation was simulated. The total network resistance calculated based on DC signal injection drops significantly upon occurrence of metallic earth-fault, as shown in Fig. 3.

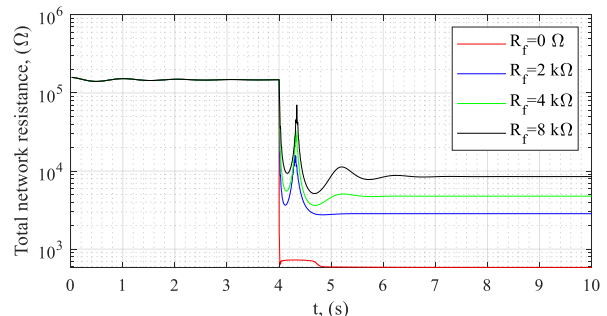


Fig. 3 Total network resistance calculated based on DC signal injection for several different fault resistances.

In case of a metallic earth fault, it drops to 854  $\Omega$ , which is actually the equivalent resistance of IVTs' primary windings. Simulation confirmed the phase voltages rise in healthy phases, from phase value of 8.16 kV<sub>p</sub> to line value of 14.14 kV<sub>p</sub>. Regardless of the fault location, the total capacitive fault current at 50 Hz ( $3I_0$ ) equals 36 A for the case without the ring connection. The injected signal amplitude in the fault current also doesn't depend on the fault location, but it depends on the AC voltage applied to the primary windings of IVTs, which can be increased if needed for detectability. For example, for 100 V, 300 V and 500 V injections, the 2.5 Hz component in the zero-sequence current reaches 0.01 A, 0.1 A and 0.25 A respectively. In terms of signal detectability, the 500 V injection would be high enough and preferred among these three options. However, for higher signal generator voltages, there is a risk for IVTs' core saturation. The magnetization curve of the considered 10 kV IVT reaches the knee point at flux value of

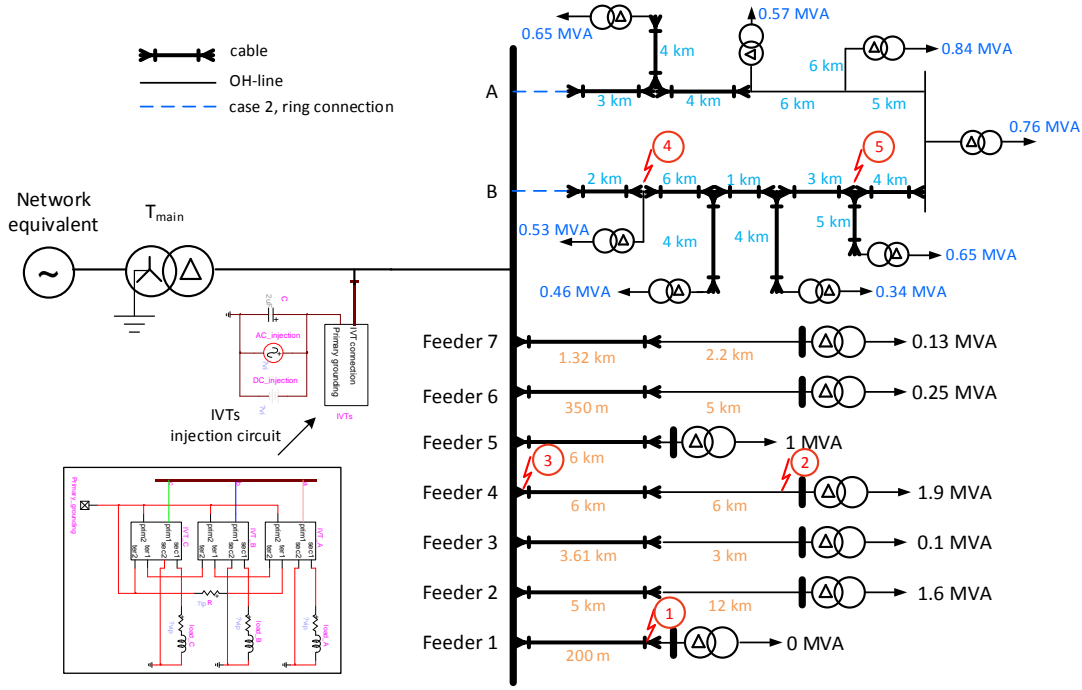


Fig. 2. Unearthed distribution network model for signal injection method simulation. Two topologies are considered – case 1 without the ring connection and case 2 with ring connection.

55 Wb, which leads to distortion of the primary current. Fig. 4 shows primary currents for different signal generator voltages. It can be observed that the saturation and distortion of primary winding currents occurs for 300 V and 500 V injections, and it is more severe after the fault occurrence. Since 100 V injection leads to hardly detectable 2.5 Hz component in zero-sequence current, the IVT could be adjusted to enable the signal injection in this particular network.

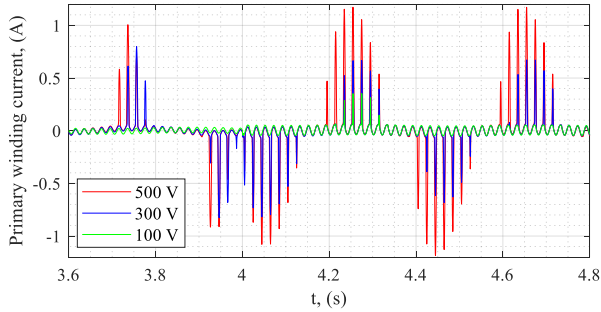


Fig. 4. Primary winding voltages in cases when signal generator produces 100 V, 300 V and 500 V. 300 V and 500 V injections lead to IVT saturation.

#### A. IVT design considerations

In order to avoid IVT saturation, the original 10 kV IVT's magnetization curve should be adjusted. Fig. 5 shows the original magnetization curve of the initially modelled IVT and three possible variations of magnetization curves. Curve 1 has increased knee point, curve 2 has a different slope, but the knee point is achieved at the same flux value as for the original curve. Curve 3 combines changes in both the slope and the flux value at knee point. These curve characteristics can be achieved by changing the core characteristics.

The increase of the cross-section will lead to the increase of

the flux at the knee point and adding one or more air gaps in the main magnetic circuit will change the curve slope.

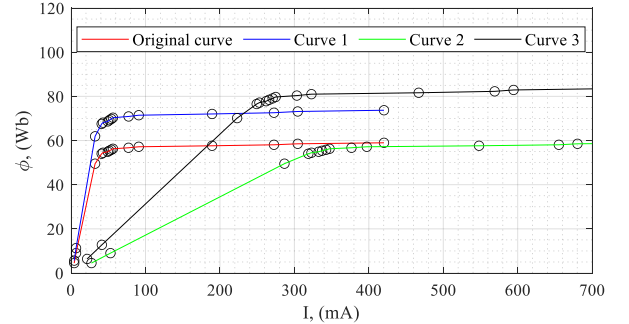


Fig. 5. IVT's original magnetization curve and proposed curve variations

The baseline condition for recalculation of the original curve is to preserve the saturation conditions in the iron core (i.e. flux density  $B$  and magnetic field strength  $H$ ). The  $B$  and  $H$  are calculated based on  $U$ ,  $I$  points from the original magnetization curve following the equations (2) and (3):

$$B = \frac{E_{rms}}{4.44 \cdot f \cdot N \cdot S} \quad (2)$$

$$H = \frac{N \cdot I}{l} \quad (3)$$

where  $E$  and  $I$  are the voltage-current pairs from original curve points,  $N$  is the number of turns,  $S$  is the core cross-section and  $l$  is the average length of a circulating magnetic field. New voltage points are obtained based on equation (2), preserving the values of  $B$ , while new current points are obtained according to equation (3) with the addition of air gap in case of curve 2 and curve 3:

$$I = \frac{H \cdot l}{N} + \frac{B}{d \cdot \mu_0} \cdot \sqrt{2}N \quad (4)$$

where  $d$  is the air gap length and  $\mu_0$  is the vacuum relative permeability. Curve 1 is obtained by increasing the cross-section from the original 24 cm<sup>2</sup> to 30 cm<sup>2</sup>. Curve 2 is achieved for cross-section of 30 cm<sup>2</sup> with the addition of 2 mm air gap. The curve 3 is achieved for further increase of the cross-section to 34 cm<sup>2</sup> and the air gap of 1.5 mm. These construction changes are not significant, and they can be easily achieved.

In case of curve 2 and curve 3 the magnetization current increases, which could worsen accuracy class of IVT or lead to winding overheating. Considering that, it is additionally possible to reconstruct the primary winding and consider conductors of larger cross-section. The winding reconstruction would solve the overheating problem and reduce the accuracy affection, so a transformer with such changes would be in its original accuracy class.

The simulation of signal injection was repeated using the proposed three curve variations. Fig. 6 shows the comparison of primary winding current in case of signal injection of 500 V and metallic earth-fault at 4<sup>th</sup> s.

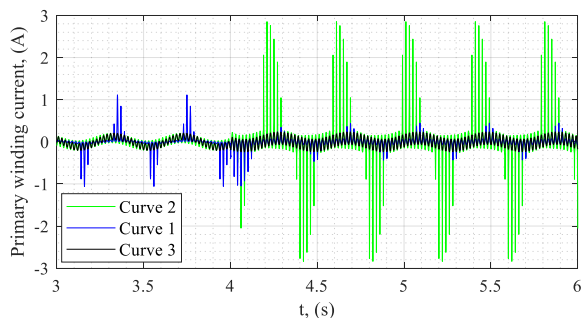


Fig. 6. Primary winding currents during the 500 V signal injection for different magnetization curves

It is obvious that curve 3 is suitable for application in the considered network since there is no saturation prior or after the metallic earth-fault occurrence. The proposed alternative magnetization curve 3 necessitates optimization of the active part of the IVT. However, it will not influence its function, final dimensions or other performance characteristics in a tangible way. Thus it can be considered realistic for construction and application as both measuring device and device for signal injection in the particular network.

### III. SIMULATION RESULTS USING THE NEW IVT CORE PARAMETERS

Since curve 3 is proven to be suitable for signal injection according to the initial simulations, the further calculations are done with magnetization curve 3 included in the IVT model. Firstly, the mixed cable-OHL network without the ring connection was considered. In such network, simulations on the feeders with the smallest and with the greatest capacitance were done. Additionally, an intermittent fault was simulated on OHL. Afterwards, the ring connection was included in the model. Ring connection influence on fault detection in radial part of the network was analysed as well as the possibility to detect the fault that occurs on the ring.

#### A. Results without the ring connection

Without the ring connection, the network consists of 7 radial feeders. The feeders' capacitive currents were calculated at 50 Hz and 2.5 Hz (Table I). The zero-sequence voltage used for calculation differs for 50 Hz and 2.5 Hz. According to Table I, feeder 1 has lowest capacitive feeder current, and feeder 4 the highest. Even though feeder 4 is not the longest one, it consists of a high cable length.

TABLE I  
INDUCTIVE VOLTAGE TRANSFORMER DATA

	50 Hz		2.5 Hz	
	$C_{tot} [\mu F]$	$X_{ctot} [k\Omega]$	$I_{Ctot} [A]$	$I_{Ctot} [mA]$
Feeder 1	0.058	54.909	0.155	1098.2
Feeder 2	1.521	2.093	4.066	41.9
Feeder 3	1.062	2.999	2.838	60.0
Feeder 4	1.764	1.805	4.713	36.1
Feeder 5	1.740	1.830	4.650	36.6
Feeder 6	0.131	24.240	0.351	484.8
Feeder 7	0.383	8.320	1.023	166.4

Simultaneous signal injection and metallic earth-fault at 2 s were simulated. Fig. 7 – Fig. 11 show results related to the IVTs: the waveforms of primary, secondary and tertiary currents, and the magnetic flux in the core.

The 2.5 Hz and 50 Hz frequencies can be observed in all waveforms. The flux does not exceed 76 Wb and there is no IVT saturation. The currents in primary, secondary and tertiary windings do not exceed 230 mA<sub>p</sub>, 2.2 A<sub>p</sub> and 4.8 A<sub>p</sub> respectively, which is under the rated continuous thermal current limits of the original IVT.

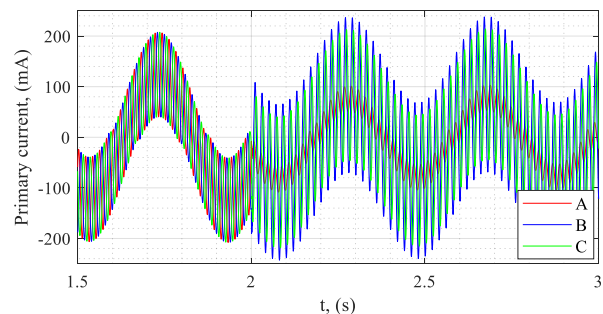


Fig. 7. Primary winding currents during the 500 V signal injection in case of metallic earth-fault that occurs at 2 s in phase A at the end of feeder 1. The primary currents reach maximal value of 230 mA after the fault.

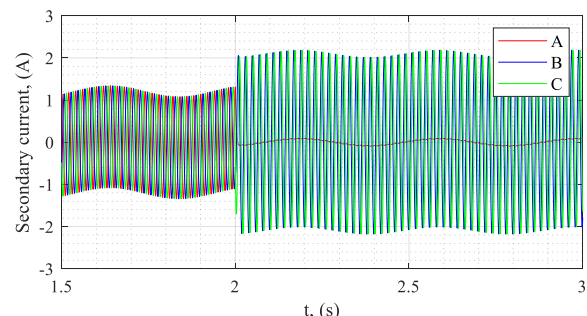


Fig. 8. Secondary winding currents during the 500 V signal injection in case of metallic earth-fault that occurs at 2 s in phase A at the end of feeder 1. The secondary currents do not exceed 2.2 A.

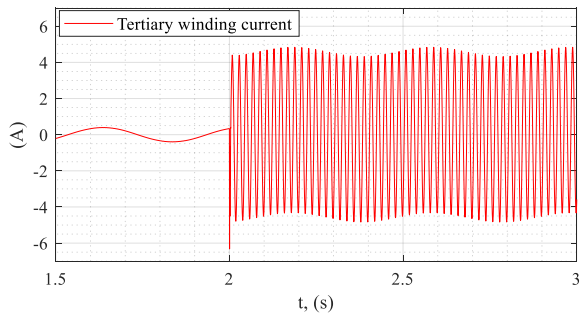


Fig. 9. Current in the delta connected tertiary windings circuit during the 500 V signal injection in case of metallic earth-fault that occurs at 2 s in phase A at the end of feeder 1. The secondary currents do not exceed 2.2 A.

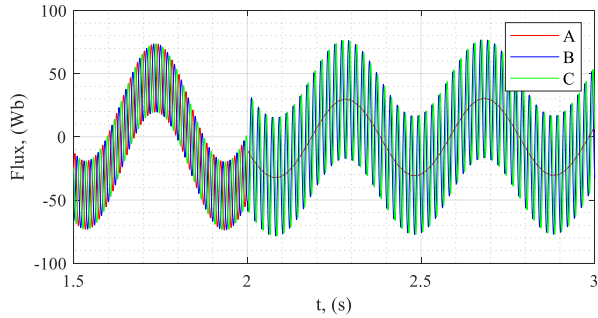


Fig. 10. Magnetic flux in the iron core of IVTs in case of metallic earth-fault that occurs at 2 s in phase A at the end of feeder 1. The flux does not exceed 76 Wb.

Fig. 11 shows the 2.5 Hz component of the residual  $3I_0$  current, measured at the beginning of each of the 7 feeders in case of fault 1. The 2.5 Hz component in residual current is calculated based on moving window of 2.5 Hz, hence the deviations during the first 0.4 s and 0.4 s after the fault occurrence in Fig. 11 should be ignored.

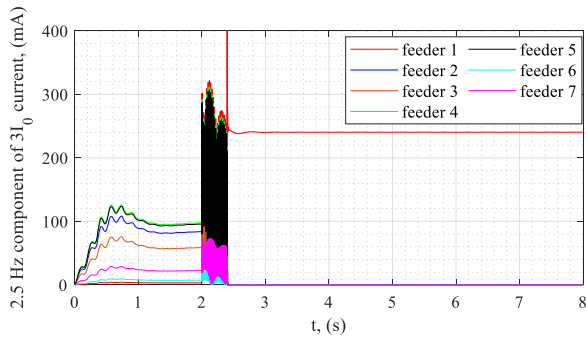


Fig. 11. 2.5 Hz component of residual currents on all feeders in case of metallic earth-fault that occurs at 2 s in phase A at the end of feeder 1. The injected 2.5 Hz signal is traceable in residual current and it is the highest one on the faulty feeder.

It can be observed that prior to the fault, all feeders have some portion of 2.5 Hz component in the residual current due to the existing injection. These values can be measured in a real network and considered as a baseline measurement for future comparison. Since the value of the 2.5 Hz component prior to the fault is proportional to the feeder capacitance, feeder 4 has the highest value of the injected 2.5 Hz signal, followed by feeder 5 and feeder 2. After the fault occurrence, the distribution of the injected 2.5 Hz signal changes. At faulty feeder, it rises to 240 mA and simultaneously drops in at all other feeders. This

proves that the 2.5 Hz is traceable to the faulty feeder.

After the simulation of metallic fault, the simulations with higher fault resistances were done. In [3], a statistical analysis showed that in unearthed network, resistances in range 20  $\Omega$  to 400  $\Omega$  and 1 k $\Omega$  to 600 k $\Omega$  occur. Fault resistance in range 30-40  $\Omega$  occurred most of the times. Additionally, it is stated that 67 % of the disturbances are intermittent faults that can be self-extinct. Fig. 12 shows the results of simulating fault 1 (end of feeder 1) with fault resistances from 0  $\Omega$  to 50 k $\Omega$ . Each colour depicts 2.5 Hz component of  $3I_0$  current measured at the beginning of each feeder, and the change in injected signal distribution in the network with raising fault resistance can be observed. At 10 k $\Omega$ , it can still be concluded that feeder 1 is the faulty one, but at 15 k $\Omega$ , due to the total impedance to ground of each feeder, the distribution is such that the injected signal can not serve for the faulty line determination. Fig. 13 shows the same simulations performed in case of fault 2 (end of feeder 4). Since the capacitance of feeder 4 is initially higher than the capacitance of feeder 1, it is expected that the detection limit for the faults at the end of feeder 4 will be reached at lower fault resistances compared to case of fault 1, since the faulty feeder residual current is proportional to the difference of total network capacitance and the capacitance of the faulty line. Fig. 13 shows that the 2.5 Hz component of residual currents of feeder 4 and feeder 5 become similar in case of fault resistance of 4 k $\Omega$ . Hence, as expected, the detection limit is reached for lower fault resistances.

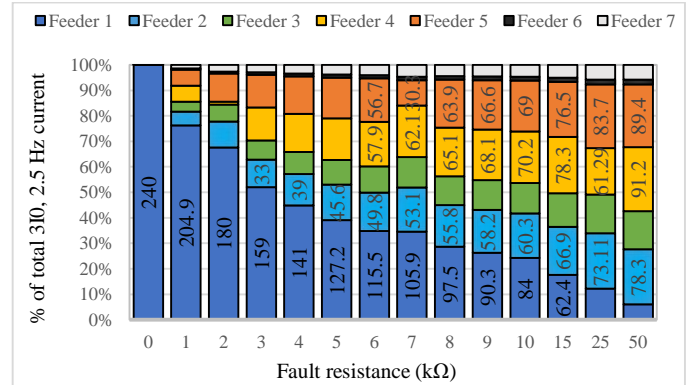


Fig. 12. 2.5 Hz component of  $3I_0$  current on feeders depending on fault resistance for the case of fault at the end of the feeder 1.

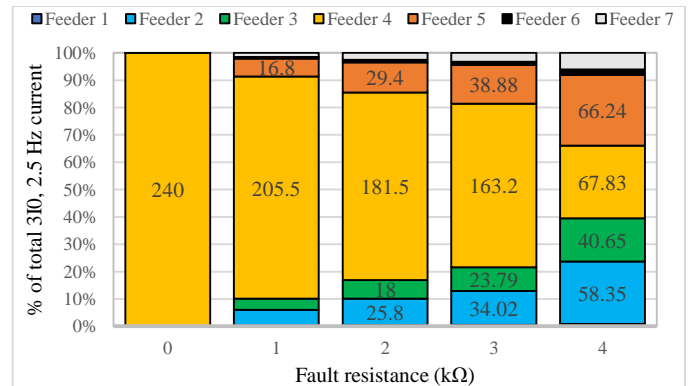


Fig. 13. 2.5 Hz component of  $3I_0$  current on feeders depending on fault resistance for the case of fault at the end of the feeder 4.

In case of fault 3, at the beginning of feeder 4, the capacitance of total feeder 4 length is not on the injected signal path. Hence

the detection limit increases for faults that occur closer to the substation. Comparing the case of fault 2 and fault 3, the detection limits are reached for fault resistances of 4 k $\Omega$  and 6 k $\Omega$ .

### B. Intermittent fault

As mentioned before, the intermittent faults can often occur in unearthed networks. Auto-extinction in unearthed network can be expected when the fault current is under 5 A [3]. For higher fault currents, the current build-up until the total breakdown is expected. To check the effect of an intermittent fault on the injection method, an intermittent fault similar to model 1 from [26] was modelled. It consists of a non-linear, time-varying resistance in series with two branches which are paralleled inversely. Each branch consists of additional resistance, DC voltage source and a diode. The time-varying resistance is based on experimental data, and it represents the build-up effect of high impedance fault current waveforms. The DC voltage sources in branches represent the arcing voltage threshold, and the diodes alongside the voltage sources guarantee the limitation of the current fault to zero when the voltage is under the breakdown values. The fault was simulated at feeder 4 on the OHL, close to the cable-OHL connection. Fig. 14 shows the fault current with obvious build-up effect and arcing effect shown in the zoomed part.

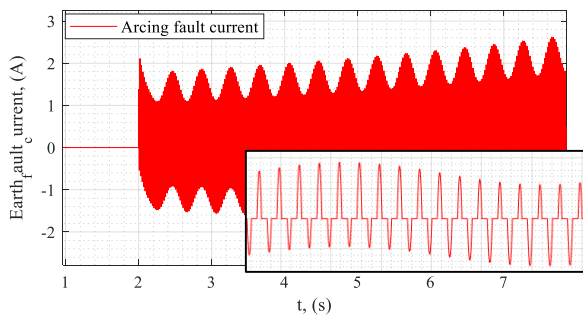


Fig. 14. Arcing fault current in case of an earth-fault at cable-OHL connection at feeder 4. During the conducting part in the fault, the fault resistance varies from 1 k $\Omega$  to 1.8 k $\Omega$ .

Fig. 15 shows the 2.5 Hz components in residual currents on all feeders. It is again observed that 2.5 Hz component is the highest on the faulty feeder and rises as the fault current builds-up, while it decreases on all other feeders. The detectability of the injected signal on the faulty feeder during the intermittent fault will in the end also depend on the fluctuations of the fault resistance.

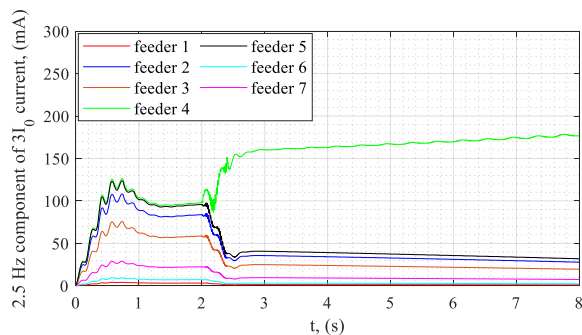


Fig. 15. 2.5 Hz component of  $3I_0$  current on all feeders during the intermittent fault from Fig. 14.

### C. Ring fault

The connection of the ring part from Fig. 2, with rather high capacitance to ground when compared to radial feeders, will change the total network capacitance and the distribution of the injected signal. Fig. 16 and Fig 17 show the injected signal distributions for faults 1 and 2. Compared to cases without the ring connection, the detection limit moves to lower fault resistances. This shows that the method performance is better in networks with capacitances to ground distributed more equal among the feeders.

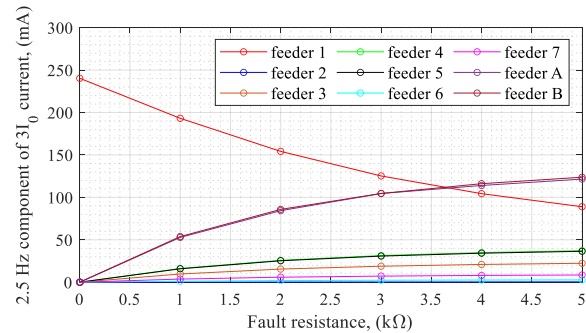


Fig. 16. 2.5 Hz component of  $3I_0$  current on all feeders in case of fault 1 with ring connection included

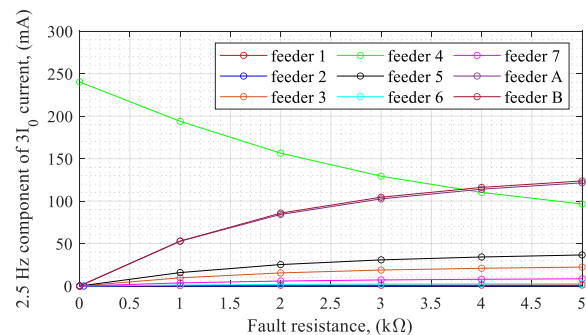


Fig. 17. 2.5 Hz component of  $3I_0$  current on all feeders in case of fault 2 with ring connection included

Regarding the detection of the earth-faults that occur on the ring, simulations of faults 4 and 5 were done. Fig. 18 shows the results in case of fault 4 – at line B, close to the substation. The injected signal in the residual current is the highest at the faulty line B up to approximately 7 k $\Omega$ . At 7 k $\Omega$ , the impedance to ground of the two paths to fault become comparable, and the injected signal is distributed equally at both paths. It becomes unclear if the fault happened at line A or B, however, comparing to the residual currents in the radial part of the network, it can still be concluded that the fault has occurred somewhere on the ring part.

In case of a fault 5, closer to the end of line B, the impedances to ground of both paths to the fault are similar even for the lowest fault resistances. Without further analysis, the faulty line is unknown. However, it can again be concluded that the fault occurred somewhere on the ring.

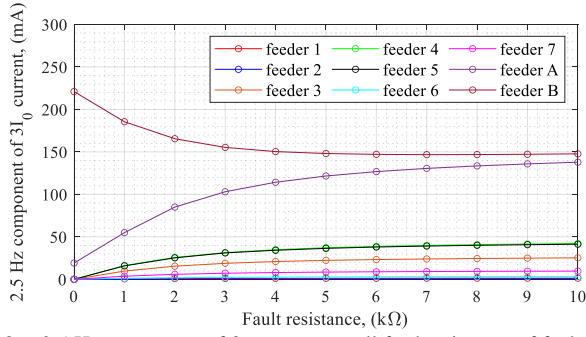


Fig. 18. 2.5 Hz component of  $3I_0$  current on all feeders in case of fault 4, at the beginning of B line in the ring

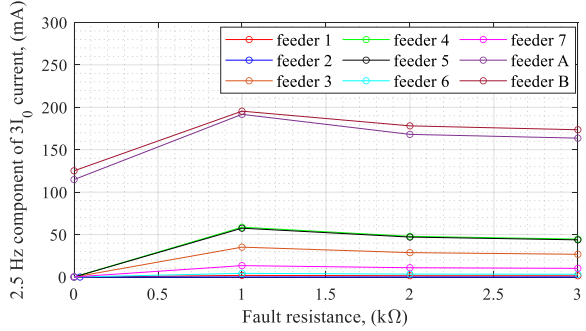


Fig. 19. 2.5 Hz component of  $3I_0$  current on all feeders in case of fault 5, at the end of the B line in the ring

#### IV. CONCLUSION

Application of signal injection method in MV distribution network was simulated on an example of a mixed distribution network with radial feeders and one ring connection. The low frequency test signal was injected using the primary windings of three single-pole insulated IVTs. The research presented in the paper gives the following conclusions:

1. IVTs can be used for signal injection in unearthened MV networks.
2. It is possible to influence the IVT design in order to achieve higher injected signal amplitudes and avoid the IVT saturation. The changes in IVT design that were done for application in the presented network would not influence its function, outer dimensions or other performance characteristics in a tangible way and the core changes that are proposed are considered realistic for construction and application.
3. The detection limit regarding the high resistance faults depends on the capacitance to ground distribution of feeders. It will be different for each network depending on the network type and topology.
4. The method performance and limits, and requirements for IVT design can be calculated and checked by simulations for any particular network. Modelling the IVT and all equipment with high capacitance to ground is essential for earth-fault and injection simulation. The IVT saturation is to be checked in order to influence the IVT design if needed, and fault at the feeder with smallest capacitance is critical to check the method limitation regarding the detection of high impedance faults.
5. When not auto-extinct, intermittent faults are detectable,

especially if there is a fault current build-up effect.

6. If a fault occurs on the ring part, in cases when the fault occurs closer to any of the ring ends, it can be concluded which part is faulty. In cases when the fault occurs at a point where it divides the ring to two parts with approximately equal capacitances to ground, it cannot be concluded which part of the ring is faulty. However, even in that case, it can be concluded if a fault occurred on the ring or elsewhere in the network.
7. The injected method is less sensitive to decrease in residual currents for faults that occur at higher distances from the substations, compared to methods that use 50 Hz components of residual currents.

#### V. FUTURE WORK

The simulations show that LF signal injection method through IVTs in unearthened network is possible and that the injected signal is traceable in the network. The plans for further research include a three-phase laboratory test setup. The test setup will consist of three-phase MV voltage source, three branches with capacitors representing the cable capacitances and a switch for earth-fault simulation. The injection circuit consisting of three IVTs and an available signal generator will be used. For proof of the concept, the currents in the circuit will be measured using shunt and available current sensors for comparison.

#### VI. APPENDIX

TABLE II  
INDUCTIVE VOLTAGE TRANSFORMER DATA

IVT winding	$U_{nRMS}$ (V)	$S_n$ (VA)	$I_{nRMS}$	$R$	$L''_{\sigma}$ (mH)	$X''_{\sigma}$ (mΩ)
Primary	$10500/\sqrt{3}$		8.25 mA	1753.1 Ω	0.75	235.82
Secondary	$10500/\sqrt{3}$	50	0.87 A	126.6 mΩ		
Tertiary	100/3	25	0.75 A	166.3 mΩ	0.36	111.71

TABLE III  
DISTRIBUTION NETWORK DATA DATA

Network data	
Main transformer	100 MVA, 132/10.5 kV, Ygd1 EMTP library model with typical inductance and resistance values
Load transformers	2 MVA, 10.5/0.4 kV, Dyd1 EMTP library model with typical inductance and resistance
Loads	Constant PQ loads, EMTP library model
Cables	3-phase PI models, $R=0.41 \Omega/km$ , $X_L=0.11 \Omega/km$ , $C=0.29 \mu F/km$ , $G=1.052e-14 S/m$
OHL	3-phase PI models, $R=0.077 \Omega/km$ , $X_L=0.34 \Omega/km$ , $C=5.976 \mu F/km$ , $G=37.55e-12 S/m$
Fault	Ideal switch + resistance for permanent fault intermittent fault model logic using diodes and different resistances depending on the voltage half-period and additional resistance for build-up of fault current waveform

#### VII. REFERENCES

- [1] C. Prévé, Protection of Electrical Networks, ISTE Ltd, 2006
- [2] T. A. Zerihun, T. Treider, H. Taxt, L. B. Nordevall, T. S. Haugan "Two novel current-based methods for locating earth faults in unearthened ring operating MV networks", *Electric Power System Research* 213 (2022) 108774

- [3] S. Hänninen, "Single phase earth faults in high impedance grounded networks-characteristics, indication and location, VTT Publ. 453 (2001), 139 p.
- [4] A. Farughian, L. Kumulainen, K. Kauhaniemi, "Review of methodologies for earth fault indication and location in compensated and unearthed MV distribution networks", *EPSR* 154 (2018) 373-380
- [5] A. H. A. Bakar, B. Ooi, P. Govindasamy, C. Tan, H. A. Illias, and H. Mokhlis, "Directional overcurrent and earth-fault protections for a biomass microgrid system in Malaysia", *Int. J. Electr. Power Energy Syst.*, vol. 55, pp. 581–591, 2014.
- [6] J. Altonen, A. Wahlroos, "Advancements in fundamental frequency impedance based earth-fault location in unearthed distribution systems", *CIGRE 19th International Conference on Electricity Distribution*, Vienna, Austria 2007
- [7] K. Lowczowski, J. Lorenc, J. Andruszkiewicz, Z. Nadolny, J. Zawodniak, "Novel Earth Fault Protection Algorithm Based on MV Cable Screen Zero Sequence Current Filter", *Energies* 2019, 12(16), 3190
- [8] A. Farughian, L. Kumulainen, K. Kauhaniemi, "Earth Fault Location Using Negative Sequence Currents", *Energies* 2019, 12(19), 3759
- [9] A. Farughian, L. Kumulainen, K. Kauhaniemi, "Non-Directional Earth Fault Passage Indication in Isolated Neutral Distribution Networks", *Energies* 2020, 13(18), 4732
- [10] X. Lin, S. Ke, Y. Gao, B. Wang, and P. Liu, "A selective single-phase-to-ground fault protection for neutral un-effectively grounded systems," *Int. J. Electr. Power Energy Syst.*, vol. 33, no. 4, pp. 1012–1017, 2011.
- [11] M. M. Alamuti, H. Nouri, R. M. Ciric, and V. Terzija, "Intermittent fault location in distribution feeders", *IEEE Trans. Power Deliv.*, vol. 27, no. 1, pp. 96–103, 2012.
- [12] I. Xyngi, M. Popov, "Transient Directional Busbar Protection Scheme for Distribution Networks", 10th IET International Conference on Developments in Power System Protection (DPSP 2010), Manchester
- [13] M. R. Adzman, "Earth Fault Distance Computation Methods Based on Transients in Power Distribution Systems", Doctoral Dissertation 189/2014, Aalto University, Finland
- [14] N.I. Elkalashy, N.A. Sabiha, M. Lehtonen, "Earth Fault Distance Estimation Using Active Traveling Waves in Energized-Compensated MV Networks", *IEEE Transactions on Power Delivery*, Volume: 30, Issue: 2, 836 – 843, April 2015
- [15] G. Druml, G. Achleitner, W. Leitner, L. Fickert, "New single-ended earth fault distance estimation for the 110 kV and 20 kV-compensated network", *Elektrotechnik & Informationstechnik* (2018) 135/8: 567–575
- [16] Y. Li, Y. Zhang, W. Liu, Z. Chen, Y. Li, J. Yang, "A fault pattern and convolutional neural network based on single-phase earth fault identification method for distribution network", *IEEE Innovative Smart Grid Technologies - Asia (ISGT Asia)*, Chengdu, China, 2019
- [17] C. Darab, R. Tarnovan, A. Turcu and C. Martineac, "Artificial Intelligence Techniques for Fault Location and Detection in Distributed Generation Power Systems," 2019 *8th International Conference on Modern Power Systems (MPS)*, 2019, pp. 1-4, doi: 10.1109/MPS.2019.8759662.
- [18] Mirshekali, H.; Dashti, R.; Keshavarz, A.; Shaker, H.R. Machine Learning-Based Fault Location for Smart Distribution Networks Equipped with Micro-PMU. *Sensors* 2022, 22, 945. <https://doi.org/10.3390/s22030945>
- [19] G. Buïgues, V. Valverde, I. Zamora, J. Mazón, and E. Torres, "Signal injection techniques for fault location in distribution networks", *Renew. Energy Power Qual. J.*, vol. 1, no. 10, pp. 412–417, 2012.
- [20] C. Raunig, L. Fickert, C. Obkircher, and G. Achleitner, "Mobile earth fault localization by tracing current injection", 7th Int. Conf. Electr. Power Qual. Supply Reliab. Conf. Proc., pp. 243–246, 2010., Kuressaare, Estonia
- [21] C. Teng, K. Schoass, G. Druml, R. Schmaranz, M. Marketz, L. Fickert, "Evaluation of new earth fault localization methods by earth fault experiments", 22nd International Conference on Electricity Distribution, 2013, Stockholm, Sweden
- [22] Y. Bai, W. Cong, J. Li, L. Ding, Q. Lu, and N. Yang, "Single phase to earth fault location method in distribution network based on signal injection principle", *DRPT 2011 - 2011 4th Int. Conf. Electr. Util. Deregul. Restruct. Power Technol.*, no. 50807032, pp. 204–208, 2011. B. Chen, N. Yu, B. Chen, C. Tian, Y. Chen, G. Ghen, "Fault Location for Underground Cables in Underground MV Distribution Networks Based on ZSC Signal Injection", *IEEE Transactions on Power Delivery* 2020, 1-1, (10.1109/TPWRD.2020.3031277)
- [23] N. Stipetic, B. Filipovic-Grcic, I. Uglesic, A. Xemard, N. Andres, "Earth-fault detection and localization in isolated industrial MV network – comparison of directional overcurrent protection and signal injection method", *Electric Power System Research*, Vol. 197, August 2021.
- [24] T. Kelemen, "Ferroresonance In Networks With Isolated Neutral", 4<sup>th</sup> HK CIGRÉ, Group 12 – Transformers, 17.-21.10.1999., Cavtat, Croatia
- [25] P. Ferracci, Groupe Schneider - Cahier Technique n°190, "Ferroresonance", March 1998.
- [26] V. C. Nikolaidis, A. D. Patsidis, A.M. Tsimtsios, "High Impedance fault modelling and application of detection techniques with EMTP-RV", *The Journal of Engineering*, 1-16, July 2018